Heliyon 10 (2024) e29482

Contents lists available at ScienceDirect

Heliyon

journal homepage: www.cell.com/heliyon

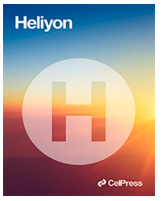

Research article

Quantitative analysis of noninvasive deep temporal interference stimulation: A simulation and experimental study

Zohre Mojiri, Amir Akhavan, Ehsan Rouhani *, Sayed Jalal Zahabi

Department of Electrical and Computer Engineering, Isfahan University of Technology, Isfahan, 84156-83111, Iran

ARTICLE INFO

Keywords:
Noninvasive deep brain stimulation
Tamporal interference
Hodgkin-Huxley model
Rat's motor cortex

ABSTRACT

Background: Deep brain stimulation (DBS) is a method for stimulating deep regions of the brain for the treatment of various neurological and psychiatric disorders such as depression, obsessive-compulsive disorder, addiction, and Parkinson's disease. Generally, DBS can be performed using both invasive and non-invasive approaches. Invasive DBS is associated with several problems, including intracranial bleeding, infection, and changes in the position of the electrode tip. Temporal interference (TI) stimulation is a non-invasive technique used to stimulate deep regions of the brain by applying two high-frequency sinusoidal currents with slightly different frequencies.

New method: This paper presents insights into the response of the spiking in the Hodgkin-Huxley (HH) neuron model of the rat somatosensory cortex by changing the parameters carrier frequency, current ratio, and difference frequency of TI stimulation. Furthermore, in order to experimentally evaluate the effect of TI stimulation on the activation of the left motor cortex, an experiment was conducted to measure the motion induced by the balanced and unbalanced TI stimulation. In the experiment, a three-axis accelerometer was attached to the right hand of the animal to determine the position of the hand.

Results: Simulation results of the HH model showed that the frequency of the envelope of the TI stimulation is identical to the fundamental frequency of the neuron spikes. This result was obtained for difference frequencies of 6 Hz and 9 Hz in balanced and unbalanced TI stimulations. Moreover specifically, when the difference frequency is set to zero, the carrier frequency is within the range of 1300–1400 Hz, and the current range is between 140 and 250 $\mu A/cm^2$, the firing rate reached to its highest value. In the experimental result, the maximum range of movement at a difference frequency of $\Delta f = 6$ Hz was approximately 1.6 mm and 5.3 mm in the z and y directions respectively.

Comparison with existing method: The results of the spatial spectrum of the rat hand movement were consistent with the spectrum information of the simulation results. Additionally, steering the interfering region to the left motor cortex leads to noticeable contralateral movement of the right hand while no movement was observed in the right hand during the stimulation of the right motor cortex.

Conclusion: This technique of stimulation for the deep regions of the brain is a promising tool to noninvasively treat various neurological and psychiatric disorders such as morphine dependence in addicted rats.

* Corresponding author.
E-mail address: erouhani@iut.ac.ir (E. Rouhani).

https://doi.org/10.1016/j.heliyon.2024.e29482
Received 17 September 2023; Received in revised form 7 April 2024; Accepted 8 April 2024

1. Introduction

Neuromodulation involves the use of various techniques to modify the activity of neurons or neural networks within the nervous system. Neuromodulation through brain stimulation involves the application of electrical currents, magnetic fields, or ultrasound waves to either excite or inhibit neuronal activity by modulating the activity of specific brain regions. Brain stimulation techniques can be used as an effective non-pharmacological approach for the treatment of diseases including depression [1], Alzheimer's [2], Parkinson's [3], and addiction [4]. This approach can be categorized into transcranial magnetic stimulation (TMS) [5], transcranial electrical stimulation (tES) [6], transcranial ultrasound stimulation (TUS) [7], and invasive deep brain stimulation (DBS) [8]. TMS is a non-invasive brain stimulation technique that uses magnetic fields to induce electrical currents in specific regions of the brain, leading to the activation or modulation of neural circuits [5]. Repetitive TMS has demonstrated efficacy in enhancing motor and cognitive abilities and alleviating depressive symptoms across various conditions such as stroke [9,10], Parkinson's disease [11], and major depressive disorder [12,13]. Similarly, tES is a noninvasive brain stimulation method that uses an electrical current to modulate neural activity in cortical regions [6]. tES can be used as an effective therapeutic technique and non-drug approach for patients suffering from alcohol abuse [14], chronic pain [14], and epilepsy [15]. Despite the multiple applications of TMS and tES, the challenges persist in stimulating deeper brain structures due to the limitations of restricted penetration depth [5] and limited targeting precision in these techniques. Therefore, DBS may be an alternative method for stimulating deeper regions of the brain. Generally, DBS can be performed using both invasive and non-invasive approaches [8]. Invasive DBS requires the implantation of electrodes in the brain to reach the targeted deep brain regions [16]. Animal studies have shown promising results in using DBS to modulate brain circuits involved in addiction-related behaviors [4,17,18]. DBS is a well-established treatment for movement disorders such as Parkinson's disease to reduce the inhibition of the motor cortex in nonhuman primates by disrupting pathological neural activity [19]. Moreover, in recent years, several human studies have shown the effectiveness of this technique to provide symptom relief for other movement disorders such as essential tremor [20], and dystonia [21]. However, invasive DBS is associated with several complications, including intracranial bleeding, infection, and changes in the position of the electrode tip [22]. Recently, to eliminate the risks associated with invasive methods, non-invasive DBS has been proposed to stimulate different deep brain areas [23]. The method does not require surgery or the placement of electrodes inside the brain, thus reducing the risk of complications associated with invasive DBS.

Temporal interference (TI) stimulation is one of the non-invasive DBS techniques that can be used transcranially to stimulate deep regions of the brain by applying two or more high-frequency sinusoidal currents with slightly different frequencies [24–26]. This technique has been clinically investigated for its effectiveness in selectively stimulating brain areas in human subjects (reduce apnea-hypopnea events in a subgroup of female patients with obstructive sleep apnea [27], enhancement of hippocampal activity and memories in individuals [28], improved motor skill learning performance through striatal stimulation [29], improvement of motor function in humans [30]) and animal models (Control of the seizure-like events by the orientation of the electrodes to focus on the hippocampus [7,31], activation of the mouse motor cortex [24]). Recently, Missey et al. developed a wireless DBS method using light-driven organic photocapacitors and laser-driven TI to selectively stimulate the hippocampus of mice while avoiding off-target stimulation in the cortex. This approach holds promise for DBS without implanted electrodes, allowing for greater mobility in animal experiments and clinical applications [32]. From the clinical point of view, one important challenge facing the selective activation of deep regions of the brain through TI stimulation is to determine the appropriate electrode placement and adjust the parameters of the stimulation. The parameters include the difference frequency, amplitudes, and current ratio of the two sinusoidal stimulations. To resolve this challenge, in the literature the macroscopic conductivity models of the brain have been developed [24,25,33–37]to examine how the field is distributed in the brain through TI stimulation. In these studies, the brain tissue has been macroscopically modeled as a homogeneous or heterogeneous cylinder or sphere. In Ref. [25], Karimi et al. developed homogeneous and inhomogeneous models of the brain to compute the electric field distribution generated during non-invasive DBS via TI stimulation. The results showed that the increase in the number of stimulating electrode pairs led to more control of the shape of the activated area. Based on the modeling of TI stimulation targeted deep brain region in Ref. [35], it was concluded that the selectivity ability of the TI stimulation depends on the relative magnitude of amplitude-modulated kHz electric fields (in the deep brain region). The aforementioned studies indicate that the depth of stimulation can be controlled by adjusting the arrangement of electrodes on the skull and the peak envelope modulation can be focused on particular brain regions by varying the current ratio between the electrode pairs [24]. While macroscopic models are effective in determining the intensity and distribution of the electric field within the brain model, microscopic models play an important role in the analysis of the response of neurons. Additionally, an evaluation of the precise location of the active region in the brain model is necessary to find a comprehensive understanding of the phenomenon. This finding highlights the importance of utilizing microscopic models for a comprehensive analysis of neuron behavior under a modulated TI field [38].

On a microscopic level, to investigate the response of neurons to external stimuli, it is necessary to develop mathematical models to describe the behavior of neurons as the fundamental units of the brain and nervous system. One of the widely used neuron models is the Hodgkin-Huxley (HH) model [39], which describes how the action potential is generated in nerve axons using mathematical relationships [40]. Several computational neuron models based on the original HH model have been developed to simulate different neuronal regions in the brain. Actually, these computational models were used to examine how action potentials initiate and activate neurons during different electrical stimulating approaches including invasive DBS of the nuclei brain [41–43], tES [44], and TI stimulation [25,45,46]. Due to the low-pass filtering properties of the neural membrane, the high-frequency stimulation of the brain cannot affect the neural activity of the neurons [24]. Furthermore, Pelot et al. performed research aimed at investigating the effect of high-frequency electrical stimulation (HFS) on motor nerve conduction block in mice. Their results showed that high-frequency stimulation of the neural membrane caused conduction block [47]. However, Mirzakhalili et al. examined the neural response of

the passive and full axon models to TI stimulation based on the standard HH model to test the hypothesis that neurons could respond to the low-frequency oscillating envelope rather than to the high-frequency stimuli. They showed that TI fields can stimulate deep brain neurons directly [45]. To better understand TI neurobiological mechanisms, Cao et al. studied the effect of TI stimulation on a single neuron model based on classical HH neuron to evaluate the effect of TI stimulation in this model [46]. Karimi et al. [25] presented a compartmental axon cable model to measure how neurons respond to electric fields generated at the activated area with the signal envelope. In all aforementioned works that focused on microscopically modeling the nerve behavior in response to the TI stimulation, the effects of the stimulation parameters have not been studied experimentally and quantitatively. Botzanowski et al. demonstrated the effectiveness of peripheral nerve stimulation (PNS) by cutaneous electrodes through TI stimulation of mice using flexible and conformable on-skin multielectrode arrays. The coordinates of the tip of the paw for different offset frequency with a high-angle shot at 30 frames was analyzed [48]. In Ref. [24], only the movement of the mice's hand evoked through TI stimulation via an in-frame ruler in one direction were analyzed. The main objective of this paper is to model the variation of membrane potential in response to the TI stimulation with different parameters and additionally to experimentally evaluate the interfering electrical induced motion in the forelimb of a rat. To this end, at first, the membrane voltage of the HH neuron model with and without TI stimulation is simulated and the effects of changes in stimulation parameters on the response of the spiking behavior of the model are investigated. Furthermore, in order to experimentally evaluate the forelimb movement in response to the unbalanced and balanced TI stimulation of the motor cortex, a three-axis accelerometer is attached to the right hand of the rat and the movement acceleration is measured in x, y and z directions. Using the three directional measured data, oscillating motion of the rat's hand is compared with the spiking patterns of the modeled neuron in the frequency domain. Additionally, the sensitivity of the rat's hand movements to the TI stimulation parameters is assessed in three directions.

This paper is organized as follows. Section 2 details the methods including the TI method, HH model equations, and experimental setup. The simulation results of the HH neuron model in response to TI stimulation with different parameters are presented in Section 3. Section 4 provides the experimental results of the effect of TI stimulation on the activation of the rat's motor cortex and finally, Sec tion 5 present s the discussion and conclusions of the study.

2. Methods

2.1. Temporal interference (TI)

TI is a non-invasive stimulation technique that utilizes the low frequency beat formed due to the superposition of two similar high frequency fields to stimulate deep regions of the brain. Therefore, if two electric fields are applied at high frequencies with a small difference frequency, the effective interference of these two applied fields can be able to follow the envelope modulation that oscillates at the difference frequency. In TI stimulation, two paired electrical currents are applied at high frequencies f_1 and $f_2 = f_1 + \Delta f$ outside the range of normal neural activity. Thus, the deep neurons receive the stimulation with the modulation of the envelope of interfering electrical fields at Δf frequency. The amplitude of the envelope modulation is controlled by the amplitudes of the two sinusoidal electric currents applied noninvasively. Moreover, the location of the envelope modulation depends on the position of the stimulation electrodes and the current amplitude ratio of the two stimulations [49].

2.2. Hodgkin-Huxley (HH) model

Electrical activity in neurons is generated and propagated using ionic (sodium (Na+) and potassium (K+)) currents through the neuron membrane. The difference between the concentrations of these ions inside and outside of the cell is the primary factor that controls the activity of the nervous system. To create the electrochemical gradients and drive the ions through the membrane, the nerve membranes contain voltage-gated ion channels so that each ion can pass through specific channels. Indeed, the ion channels across the membrane serve as conductors of ionic currents between intracellular and extracellular spaces and make the electrical potential across the membranes of nerve cells. To transmit the nerve signals along the nerve membranes, the membrane voltage changes rapidly from the rest (negative) value to the positive along the nerve fiber called the action potential. The mechanism of an action potential is that when the voltage of the membrane reaches the threshold level, the membrane suddenly becomes very permeable to sodium ions, and the ions in a high concentration flow from extracellular to intracellular using the fast sodium channels (depolarization phase). At the overshoot of the action potential, the sodium channels are closed and the voltage of the membrane returns to the initial value (rest) with the permeation of the potassium ions from the intracellular space to the extracellular space (repolarization phase). To better understand the mechanism of the action potential, Hodgkin and Huxley presented the nonlinear dynamic model originated from the pioneering experiments conducted on the axon of a squid giant. This model has become one of the most important models in computational neuroscience, describing the generation and propagation of action potentials in neurons. Over the years, the original Hodgkin-Huxley (HH) model has been adapted and modified to study the mechanism of the action potential in neurons of the rat cortex [50]. The developed HH-type neuron models of the rat cortex aim to capture the specific electrical properties and characteristics of cortical neurons. In the current paper, the HH-type model of regular spiking in cerebral cortex developed in Ref. [50] based on in vivo and in vitro electrophysiological recordings from rat somatosensory cortex is used to evaluate the effect of TI stimulation with different parameters on membrane voltage of the neuron. The dynamic equations of the model in equations (1)–(5) are as follows:

$$C_m\frac{dV}{dt}=I-g_{leak}(V-E_{leak})-I_{Na}-I_K-I_L-I_M \tag{1}$$

where in equation (1), V is the voltage of the membrane, C_m denotes the specific capacitance of the membrane, g_{leak} represents the resting (leak) membrane conductance, and E_{leak} is the reversal potential associated with the leakage current. The parameters I_K, I_{Na}, and I_L are the currents for potassium, sodium, and high threshold calcium current, respectively. I_M is a slow voltage-dependent potassium current involved in spike-frequency adaptation and I is an external current applied to the membrane of the neuron. The voltage-dependent Na^+ current is represented with the following equation:

$$I_{Na}=\overline{g}_{Na}m^3h(V-E_{Na})$$

$$\alpha_m=\frac{-0.32(V-V_T-13)}{\exp[-(V-V_T-13)/4]-1}$$

$$\beta_m=\frac{0.28(V-V_T-40)}{\exp[(V-V_T-40)/5]-1}$$

$$\alpha_h=0.128\exp\left[\frac{(-V-V_T-17)}{18}\right]$$

$$\beta_h=\frac{4}{1+\exp[-(V-V_T-40)/5]}$$

$$\frac{dm}{dt}=\alpha_m(1-m)-\beta_m m$$

$$\frac{dh}{dt}=\alpha_h(1-h)-\beta_h h \tag{2}$$

where in equation (2), $\overline{g}_{Na}$ and E_{Na} are the maximum conductance and Nernst potential for Na^+ and V_T adjusts the spike threshold. m is the probability of activation gates for Na^+ and h is the probability of inactivation gates for Na^+. α_i and $\beta_i, i\in\{m,h\}$ are the voltage dependence nonlinear exponential functions. The current I_K is defined in the following equations:

$$I_K=\overline{g}_K n^4h(V-E_K)$$

$$\alpha_n=\frac{-0.032(V-V_T-15)}{\exp[-(V-V_T-15)/5]-1}$$

$$\beta_n=0.5\exp\left[\frac{(-V-V_T-10)}{40}\right]$$

$$\frac{dn}{dt}=\alpha_n(1-n)-\beta_n n \tag{3}$$

where in equation (3), $\overline{g}_K$ and E_K are the maximum conductance and Nernst potential of K^+, n is the probability of activation gates for K^+ and α_n and β_n are the voltage dependence nonlinear exponential functions. A high threshold Ca^+ current is defined as follows:

$$I_L=\overline{g}_L\, q^2\, r\,(V-E_{Ca})$$

$$\alpha_q=\frac{0.055(-27-\mathrm{V})}{\exp[(-27-V)/3.8]-1}$$

$$\beta_q=0.94\exp\left[\frac{(-75-V)}{17}\right]$$

$$\alpha_r=0.000457\exp[(-13-V)/50]$$

$$\beta_r=\frac{0.0065}{\exp[(-15-V)/2]+1}$$

$$\frac{dr}{dt}=\alpha_r(1-r)-\beta_r r$$

$$\frac{dq}{dt}=\alpha_q(1-q)-\beta_q q \tag{4}$$

where in equation (4), $\bar{g}_L$ and E_{Ca} are the maximum conductance and Nernst potential of Ca^{++} and α_i and $\beta_i, i \in \{q, r\}$ are the voltage dependence nonlinear exponential functions. The slow K^+ current responsible for spike frequency adaptation is represented as

$$I_M = \bar{g}_M\, p\, (V - E_K)$$

$$p_\infty(V) = \frac{1}{1 + \exp[-(V+35)/10]}$$

$$\tau_p(V) = \frac{\tau_{max}}{3.3\exp[(V+35)/20] + \exp[-(V+35)/20]}$$

$$\frac{dp}{dt} = \frac{p_\infty - p}{\tau_p} \tag{5}$$

In equation (5), $\bar{g}_M$ and E_K are the maximum conductance and Nernst potential of K^+ and τ_{max} is the time constant of the adaptation current. The main objective of the paper is to investigate the variation of membrane potential in response to the TI stimulation as the external current and to validate the simulation results with the experimental tests.

2.3. Experimental setup

In this section, to evaluate the effectiveness of TI stimulation in the activation of neural activity at a site in the deep region of the brain, an experiment is conducted on an animal model and the movement results of the right forelimb are presented. The experiment was performed in the Medical Engineering Laboratory of the Isfahan University of Technology. All surgical procedures described in this paper were approved by the Research and Ethics Committee of Isfahan University of Medical Sciences, Isfahan, Iran (No. IR.MUI.AEC.1401.010). One male Wistar rat (247 g body weight) was deeply anesthetized by intraperitoneally administrated urethane (1.6 g/kg). The incision area of the head was shaved and the scalp was exposed along the midline. The animal was positioned in the stereotaxic (Model 941, Toos Bio-Research Co., Mashhad, Iran) setup which allows the forelimbs to hang free while the head and ears were fixed into the frame.

2.3.1. TI stimulator and data acquisition

A custom-made isolated four-channel TI stimulator was used to stimulate the surface of the skull. The simulator is a voltage-controlled current source that generates sinusoidal waves in four channels. In the current study, only two channels are applied to stimulate the brain regions. Every channel includes a Howland current source (HCS), which utilizes an operational amplifier (op-amp) in a grounded-load circuit to generate a precise and stable output current that is directly proportional to the input voltage. The stimulator is powered by a direct current (DC) power source using MINMAX converters (specifically, the mau203 Ultra Miniature High Isolation SIP DC/DC Converter) to ensure electrical isolation of the voltage supplies in each channel of the stimulator. The stimulating device receives sinusoidal voltage signals (v) through signal generators (specifically, the Leader LAG-125 Low Distortion Audio Generator, India). These voltage signals are then converted into sinusoidal current signals (mA) at the output of each channel. The output of each channel can generate either a continuous or pulsed TI signal. The pulse amplitude, ranging from −3 mA to 3 mA and the carrier frequency ranging from 1 Hz to 5000 Hz of the stimulation signal can be manually adjusted although the selectors and push buttons located on the panel of the simulator. The electric currents are applied via two pair electrodes on the positions shown in Fig. 1.

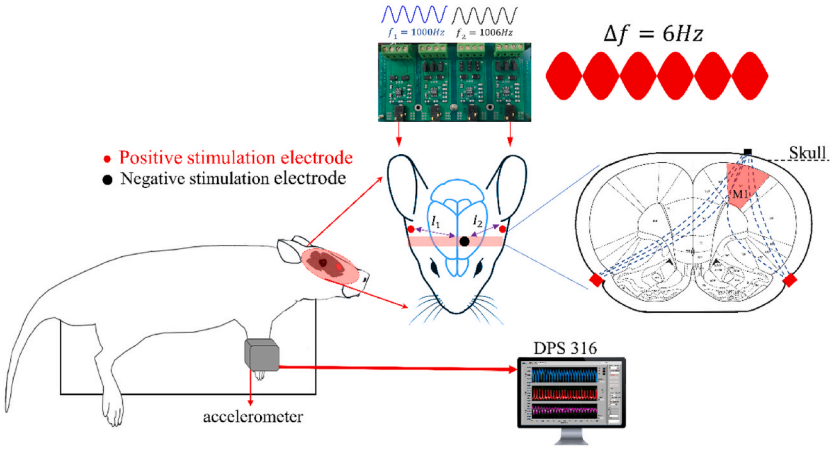

Fig. 1. A Schematic of the locations of the stimulus electrodes on the rat's head and attachment of the accelerometer to the rat's right hand. The black circle depicts the common ground skull electrode at AP = +3 mm and ML = +3 mm from Bregma and the gray circles show the paired clamp electrodes.

The common ground (black circle) electrode is placed at the coordinates anterior/posterior (AP), +3 mm and medial/lateral (ML), +3 mm according to the Paxinos atlas [51]. The ground electrode is attached to a screw on the skull with plastic holders so that only the screw tip is in contact with the skull and the holders are affixed to the skull with dental acrylic cement. The two positive electrodes (red circles) are positioned under the ears using clamp electrodes. A three-axis accelerometer (DPS 3016 Dideh Pardaz Saba Co., Isfahan, Iran) is used to quantitatively evaluate the movement of the right hand. The sensor is attached to the right hand (Fig. 1) to record the movement acceleration. The three accelerometer signals are transmitted with the sample rate of 3105.6 Hz to a custom application software written in LabVIEW on the computer through a USB interface and the data is analyzed offline using MATLAB R2019a.

3. Results

3.1. Simulation results

In this section, the membrane voltage of the HH neuron model in response to TI stimulation with different parameters is simulated. The parameters of the model for regular spiking are summarized in Table 1. The simulations are performed on a computer (Intel (R) Core (TM) i7-9700K @ 3.60 GHz CPU and 32 GB DDR4 RAM) in MATLAB R2020a Simulink. Let the TI stimulation current be $I_{TI} = I_1 \sin(2\pi f_1 t) + I_2 \sin(2\pi f_2 t)$ μA/cm^2 and the difference frequency of the stimulation be $\Delta f = f_1 - f_2$. In the first simulation the effect of electrical stimulation without temporal interference, i.e. $I_2 = 0$, is presented. Fig. 2A shows periodic bursts of spikes in response to a 6 Hz AC stimulation at 10 μA/cm^2 current density in a HH spiking neuron model. The stimulation current is illustrated in Fig. 2B. The sodium (G_{Na}), potassium (G_K), slow potassium (G_M) and calcium (G_L) conductance and their membrane currents are shown in Fig. 2C and D, respectively. It can be seen that during the depolarization phase sodium conductance (G_{Na}) increases and in the repolarization stage, the sodium conductance decreases, while the potassium conductance (G_K) increases (Fig. 2C). Additionally, the frequency spectrum of the membrane voltage in response to the single AC stimulation is illustrated in Fig. 2E. The results show that the fundamental frequency of the spectrum coincides with the stimulation frequency. Moreover, since the membrane voltage is periodic, the higher-order harmonics are also evident in the frequency spectrum.

Fig. 3 shows the effect of balanced TI stimulation, i.e. $I_1 = I_2$, for $\Delta f = 6$ Hz and $\Delta f = 9$ Hz. The neuron spikes and the TI stimulation waveform for $\Delta f = 6$ Hz are illustrated in Fig. 3A and B, respectively. It can be seen that the frequency of the envelope of the stimulation current is 6 Hz and the spiking pattern of the neuron is synchronized with the stimulation envelope. To consider the effect of difference frequency in the TI stimulation, the previous simulations were repeated for $\Delta f = 9$ Hz. The HH neuron response and the TI current waveform for $\Delta f = 9$ Hz are presented in Fig. 3C and D, respectively. Similar to the previous results, neuron firing starts from the falling stage of the TI envelope. In Fig. 3E the frequency spectrum of the membrane voltage in response to TI stimulation with $\Delta f = 6$ Hz and $\Delta f = 9$ Hz are illustrated in solid and dashed lines, respectively. The results show that the fundamental frequency of the neuron responses coincides with the difference frequency of the TI stimulation.

One of the main parameters in the TI stimulation which control the location of the interfering electric fields is the amplitude ratio, I_1/I_2. In scenarios with unbalanced TI stimulation ($I_1 \neq I_2$), the location of the interfering region moves toward the electrode pair with a lower current. In Fig. 4 the response of the HH neuron model to unbalanced TI stimulation with $I_1/I_2 = 2/3$ is presented. Fig. 4A–D illustrates the neuron responses for $\Delta f = 6$ Hz and $\Delta f = 9$ Hz and the corresponding unbalanced TI stimulation waveforms. As shown in Fig. 4E the frequency spectrum of the membrane voltage shows the peak frequencies of 6 and 9 Hz as well as their harmonics.

As presented in the simulation results in Figs. 3 and 4, to control the fundamental frequency of the neuron firing, the frequency of the stimulation envelope which is equal to the difference frequency, $\Delta f = f_1 - f_2 \neq 0$, should be adjusted. Fig. 5 demonstrates the effect of TI stimulation parameters on the firing rate of the neuron in the HH model by changing the parameters carrier frequency (ranging from 1 KHz to 2 KHz with a step size of 100 Hz), difference frequency (ranging from 0 Hz to 100 Hz with a step size of 3 Hz), and current amplitude I_1 and I_2 (ranging from 110 to 250 $\mu A/cm^2$ with a step size of 10 $\mu A/cm^2$ in balanced scenario and current ratio (I_1/I_2) from 0 to 1 in unbalanced scenario). In the results of balanced TI stimulation (Fig. 5A), when the difference frequency is set to zero, the carrier frequency is within the range of 1300–1400 Hz, and the current range is between 140 and 250 μA/cm^2, the firing rate reached

Table 1
The parameters of the HH-type neuron model of the rat somatosensory cortex for regular spiking [50].

Parameter	Value	Unit
C_m	1	$\mu A/cm^2$
g_{leak}	0.0205	mS/cm^2
$\bar{g}_{Na}$	56	mS/cm^2
$\bar{g}_K$	6	mS/cm^2
$\bar{g}_M$	0.075	mS/cm^2
$\bar{g}_L$	0.1	mS/cm^2
E_{leak}	−70.3	mv
E_{Na}	50	mv
E_K	−90	mv
E_{Ca}	120	mv
V_T	−56.2	mv
τ_{max}	608	$msec$

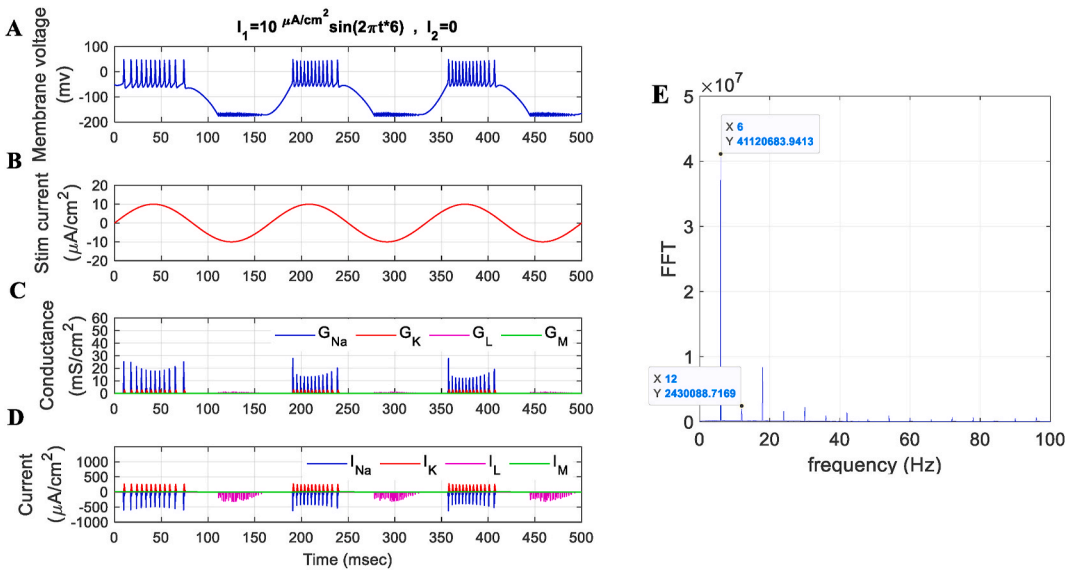

Fig. 2. Simulation results of an spiking mode neuron in the HH model with a single AC (6 Hz) stimulation current with the amplitude of 10 μA/cm^2. (A) Membrane voltage (*mv*). (B) The applied stimulation current (μA/cm^2). (C) Conductance of Na^+, K^+, slow K^+, and Ca^+ (mS/cm^2). (D) Na^+, K^+, slow K^+, and Ca^+ ionic currents. (E) Frequency spectrum of the membrane voltage.

to its highest value. As the carrier frequency and difference frequency increase, the firing rate tends to decrease (0 Hz). The interesting observation is that when the amplitude of the stimulation reached to 250 $\mu A/cm^2$, the firing rate increased from 0 Hz to 320 Hz. Fig. 5B and C showed the firing rate of the HH model in the unbalanced states for $I_1 \neq I_2, I_1 + I_2 = 300\ \mu A/cm^2$ and $I_1 \neq I_2, I_1 + I_2 = 400\ \mu A/cm^2$, respectively [52]. The results indicated the highest firing rates (720–799 Hz) for carrier frequency from 1200 to 1300 Hz, current ratio from 0 to 0.03 and Δf between 0 and 100 Hz (Fig. 5B) and for carrier frequency from 1200 to 1450 Hz, current ratio from 0 to 0.17, and Δf from 0 to 100 Hz (Fig. 5C). In contrast, for the state of $I_1 + I_2 = 300\ \mu A/cm^2$, as the carrier frequency increases to the range 1800–2000 Hz, regardless of variations in the difference frequency and current ratio, the firing rate decreases to 0–80 Hz. While for the state of $I_1 + I_2 = 400\ \mu A/cm^2$, the highest firing rate of 320–400 Hz is observed for the difference frequency in the range 30–80 Hz and carrier frequency of 2000 Hz.

3.2. Experimental results

In the first scenario, due to the position of the common ground electrode on the left hemisphere of the brain on the skull, the current ratio $I_1/I_2 = 1$ results in the envelope modulation being inclined towards the left side of the motor cortex. In this scenario, the stimulation caused a periodic movement of the right hand at different frequencies. The activation of the motor cortex, under induced TI stimulation, was recorded in a video aimed at monitoring movement at 30 fps. The stimulation is applied with intensity of $I_1 = I_2 = 1$ mA, a carrier frequency of 1 kHz and a difference frequency (Δf) of 3 Hz. Fig. 6 demonstrates the 10 shots of the movement of the right hand in 0.33 s (See movie S1 for a representative video). Fig. 7 shows the results of the effect of the difference frequency on the acceleration of the right-hand movement with the stimulating amplitude of $I_1 = I_2 = 0.75$ mA and a carrier frequency of 1 KHz. The results showed that for $\Delta f = 0$, no movement is observed (Fig. 7A–C) while the periodic movement is obtained (nonzero acceleration in three dimensions) in Fig. 7D–I for $\Delta f = 6$ and $\Delta f = 9$ Hz. The maximum amplitude of acceleration occurs in the y direction for $\Delta f = 9$ Hz (Fig. 7H).

The frequency spectrum of the acceleration in the y and z directions is depicted in Fig. 8A and B, respectively. The results show that the fundamental frequency peaks of the spectrum coincide with the difference frequency of the TI stimulation. Furthermore, similar to the simulation results, the higher order harmonics are appeared in the frequency spectrum. Fig. 9 shows the movement pattern of the rat's right hand in the Z-Y plane in response to TI stimulation with $I_1 = I_2 = 0.75$ mA [24]. The results are obtained using double integration of the acceleration signals. As shown in Fig. 9A, the maximum range of movement at $\Delta f = 6$ Hz is approximately 1.6 mm and 5.3 mm in the z and y directions respectively. Noted that for $\Delta f = 0$ Hz, the trajectories are centered on the origin (red color in Fig. 9A). In Fig. 9B, the range of movement in y and z directions at $\Delta f = 9$ Hz is approximately 3 and 0.9 mm.

In the second scenario, the results of the effect of the unbalanced TI stimulation on the rat's hand movement were investigated. By varying the current ratio between electrode pairs while keeping the sum of the amplitudes in a constant value, the peak envelope modulation was steered toward the electrode pair with the lower amplitude [17]. The displacement of the interfering region can be verified by the movement in the contralateral limb. The results for the current ratios of $I_1/I_2 = 1.5$ ($I_1 = 0.75$, $I_2 = 0.5$ mA), $I_1/I_2 = 0.66$ ($I_1 = 0.5$, $I_2 = 0.75$ mA), $I_1/I_2 = 4$ ($I_1 = 1$, $I_2 = 0.25$ mA), and $I_1/I_2 = 0.25$ ($I_1 = 0.25$, $I_2 = 1$ mA) were illustrated in Fig. 10. The results showed that there has been no noticeable movement when the amplitude of the electrodes satisfied the condition $I_1 < I_2$ for both

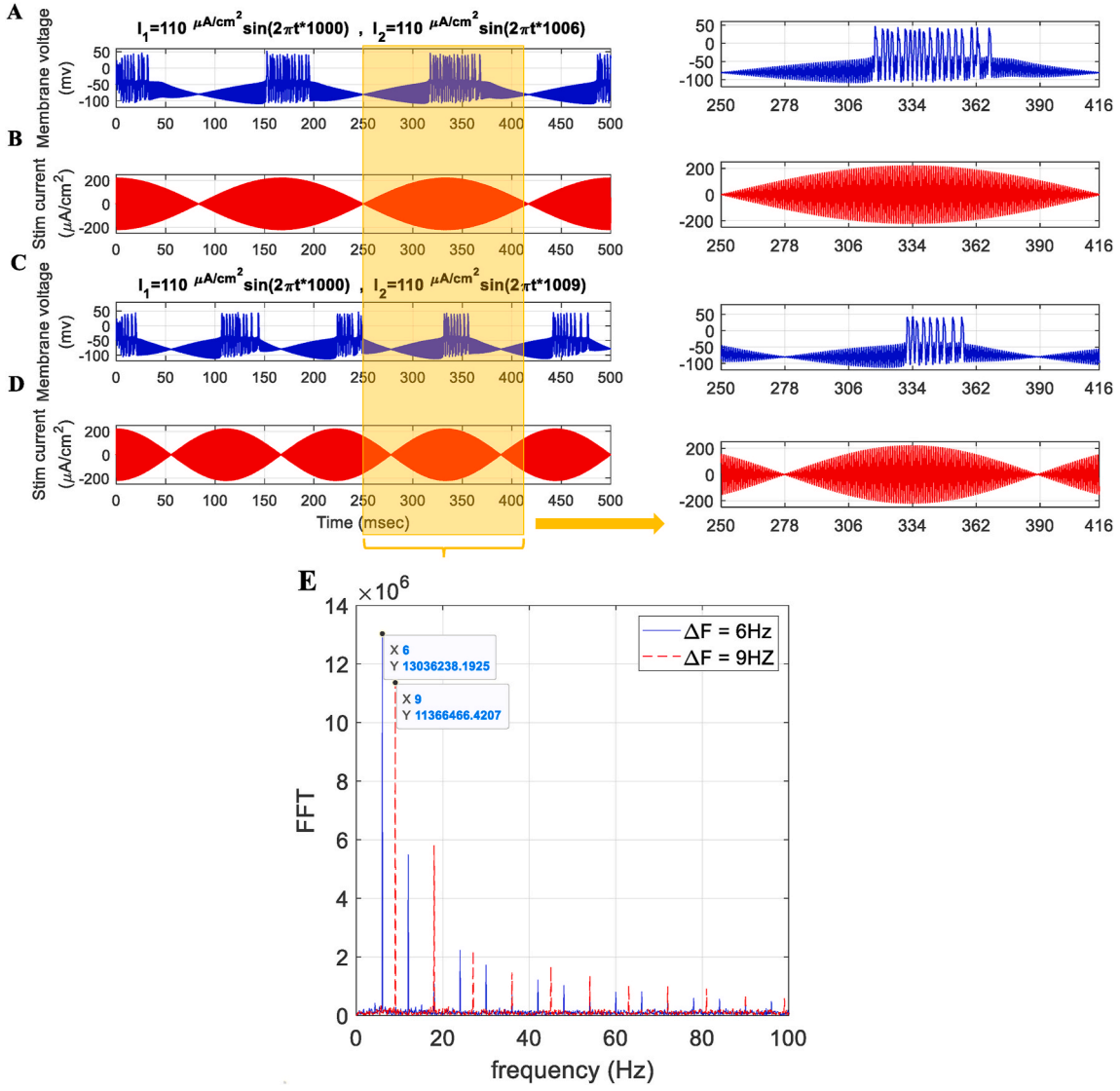

Fig. 3. Neuron response to the balanced TI stimulation in the HH model. (A) neuron spikes in response to a TI stimulation for $\Delta f = 6$ Hz. (B) The balanced TI stimulation current for $\Delta f = 6$ Hz with the amplitude of 110 ($\mu A/cm^2$). (C) Neuron spikes in response to a TI stimulation for $\Delta f = 9$ Hz. (D) The balanced TI stimulation current for $\Delta f = 9$ Hz with the amplitude of 110 ($\mu A/cm^2$). (e) The frequency spectrum of the membrane voltage in response to the TI stimulus for $\Delta f = 6$ Hz and $\Delta f = 9$ Hz.

difference frequencies of 6 and 9 Hz while for the condition $I_1 > I_2$ the movement was observed in both y and z directions for two different current ratios of 1.5 and 4. For $\Delta f = 9$ Hz, the maximum amplitude of hand movement is approximately 1 mm in the z direction and 2 mm in the y direction (Fig. 10B) and for $\Delta f = 6$ Hz the value is approximately 2 mm in the z direction and 5.5 mm in the y direction (Fig. 10D) at the current ratio of 4. The results in Fig. 10 demonstrated that with the electrodes positioned according to Fig. 2A the maximum range of movement in both y and z directions is obtained for I_1:I_2 = 1:0.25 mA and $\Delta f = 6$ Hz. The result of Fig. 10A indicates the minimum amplitude of hand movement at $\Delta f = 9$ Hz for a current ratio of 1.5 (0.55 mm in the y direction and 1 mm in the z direction). Moreover, for $\Delta f = 6$ Hz, the minimum amplitude is approximately 0.4 mm in the z direction and 0.2 mm in the y direction for a current ratio of 1.5 (Fig. 10C).

4. Discussion and conclusion

In this study, a simulation approach was employed using the developed HH neuron model (constructed based on electrophysiological recordings obtained from in vivo and in vitro experiments conducted on the rat somatosensory cortex) to assess the impact of TI stimulation by analyzing the simulated responses of the model. Subsequently, an experimental methodology was implemented to evaluate the effects of TI stimulation on the activation of motor cortex of rats. The simulation section of the paper demonstrated the

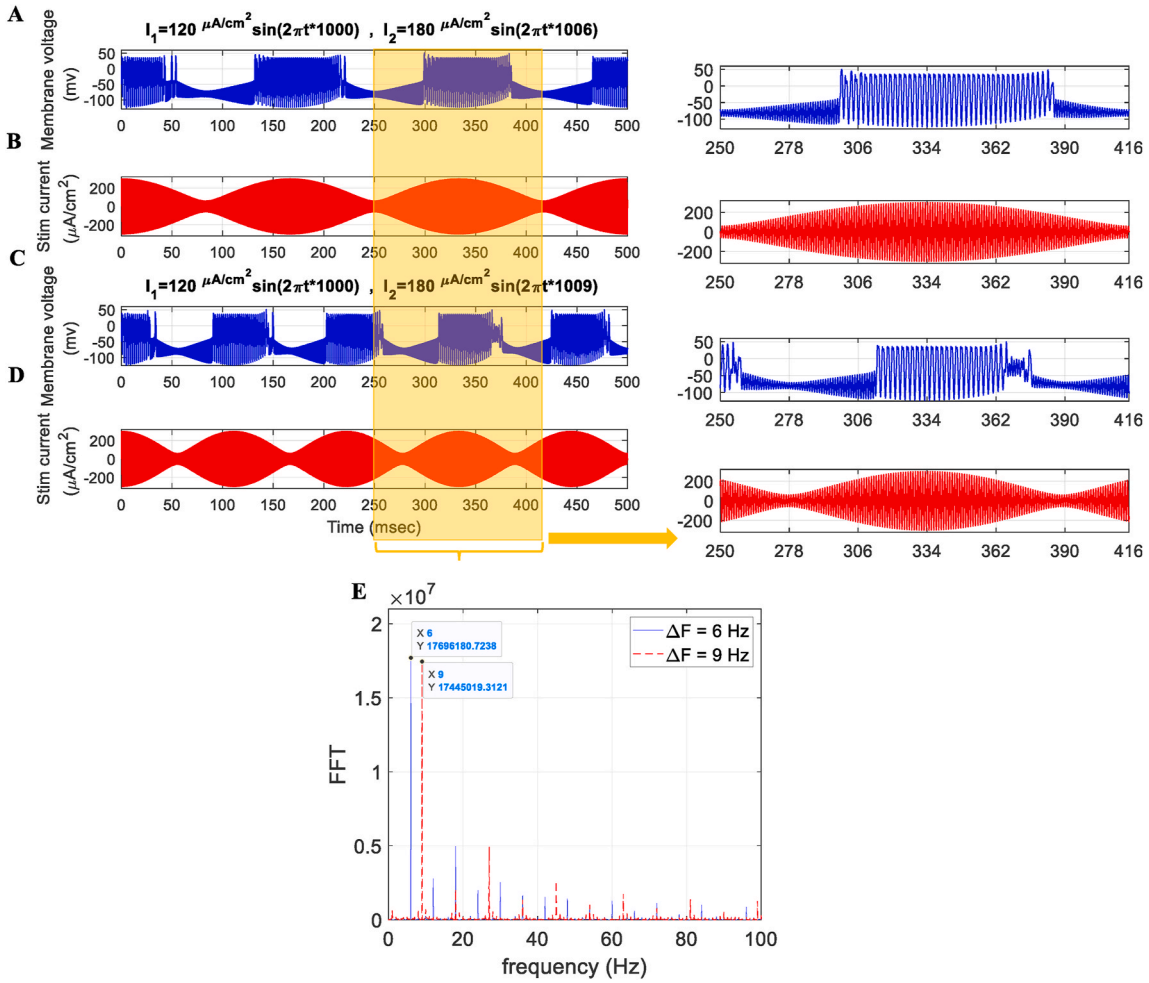

Fig. 4. (A) Neuron response to unbalanced TI stimulation current in the HH model for $I_1/I_2 = 2/3$ (a) neuron spikes in response to the unbalanced TI stimulation for $\Delta f = 6$ Hz. (B) The unbalanced TI stimulation current for $\Delta f = 6$ Hz (C) Neuron spikes in response to the unbalanced TI stimulation for $\Delta f = 9$ Hz. (D) The unbalanced TI stimulation current for $\Delta f = 9$ Hz (E) Frequency spectrum of the membrane voltage in response to the TI stimulus for $\Delta f = 6$ Hz and $\Delta f = 9$ Hz.

feasibility of the firing rate of the neuron by adjusting the difference frequency between two stimulation currents in Fig. 4A–D. The results illustrated that the neuron's firing pattern is synchronized with the envelope of the TI stimulation. Additionally, the frequency spectrum of the membrane voltage in response to the TI stimulation revealed that the fundamental frequency of the neuron's responses coincides with the difference frequency of the TI stimulation. The existence of higher-order harmonics, along with the fundamental peak, observed in the frequency spectrum as illustrated in Fig. 4E, can be attributed to the periodic behavior of the neuron in both balanced and unbalanced TI stimulations. Additionally, the current study specifically evaluated the effective parameters of frequency, amplitude, and current ratio of TI stimulation on the firing rate of the neuron in balanced and unbalanced states. Previous researches have demonstrated that neurons can exhibit different response patterns to high-frequency (kHz) stimulation [53,54]. Some neurons may exhibit an initial response to the stimulus, while others may continue firing continuously throughout the duration of the stimulation. However, Grossman et al. [24] evaluated the effects of TI stimulation on the primary motor cortex (M1) in the somatosensory cortex of anesthetized mice using in vivo whole-cell patch clamp. The results showed that applying TI stimulation using two sinusoidal currents with a carrier frequency of 2 kHz and no difference frequency did not elicit any observable neural activity within the nucleus. Moreover, the simulation results of Bhadra et al. [55] showed that high-frequency stimulation between 3 and 40 kHz can inhibit the propagation of action potentials along an axon. The results of the current study, as presented in Fig. 5A–C, demonstrated that TI stimulation with a carrier frequency ranging from 1 to 2 KHz, without any temporal interference ($\Delta f = 0$), can elicit periodic bursts of spikes in an HH spiking neuron model. In the balanced scenario (Fig. 5A), an increase in the carrier frequency, current, and difference frequency parameters resulted in a firing rate of 160–240 Hz. Increasing the carrier frequency and the intensity of the current, accompanied by a subsequent reduction in the difference frequency, resulted in a decrease in the firing rate, ranging from 0 to 80 Hz. These findings highlight the dependence of the neuron response to the difference frequency in this scenario. Nevertheless, when the carrier frequency was elevated (reduced) and the intensity was decreased (increased), spanning across frequency differences ranging

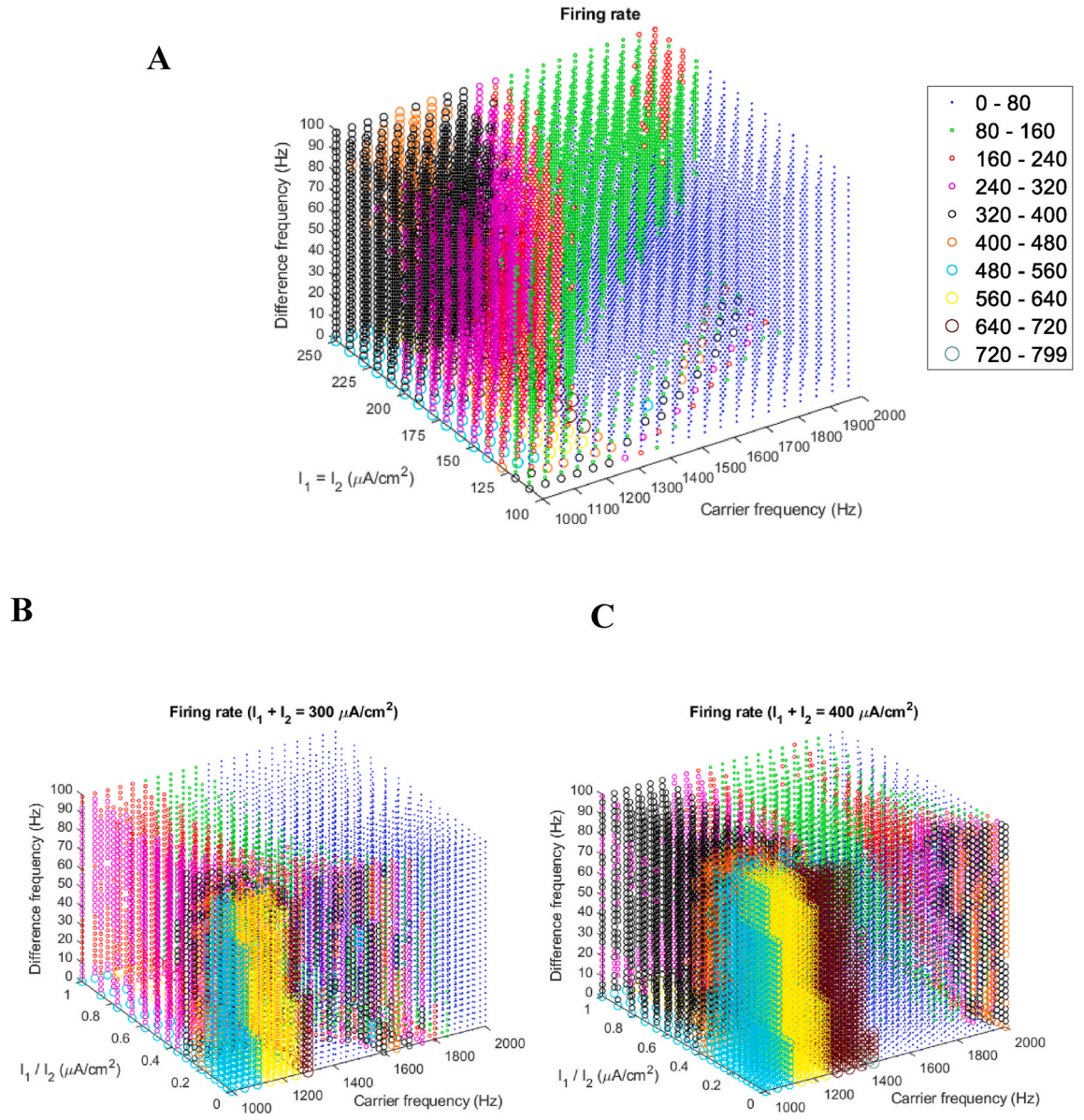

Fig. 5. The firing rate (Hz) for carrier frequencies ranging from 1 KHz to 2 KHz with a step size of 100 Hz and difference frequencies (Δf) ranging from 0 Hz to 100 Hz with a step size of 3 Hz. (A) Balanced TI stimulation for current values $I_1 = I_2$ ranging from 110 to 250 $\mu A/\ cm^2$ with a step size of 10 $\mu A/cm^2$. (B) Unbalanced TI stimulation for $I_1 + I_2 = 300\ \mu A/cm^2$ with a step size of 10 $\mu A/cm^2$ and the current ratio from 0 to 1. (C) Unbalanced TI stimulation for $I_1 + I_2 = 400\ \mu A/cm^2$ with a step size of 10 $\mu A/cm^2$ and the current ratio from 0 to 1.

from 0 to 100 Hz, the firing rate consistently remained in the range of 0–80 Hz (320–400 Hz). These findings suggest that the neuronal activity of a neuron in the balanced current scenario occurs at carrier frequencies lower than 1200 Hz. In the context of unbalanced stimulation, it was observed that raising the current ratio from zero to one, specifically at carrier frequencies below 1800 Hz, resulted a decrease of firing rate (Fig. 5B). Despite observing different responses of the model to TI stimulation with different parameters, it should be noted that the current study did not incorporate the thickness and length of the axons in the model. The thickness of axons may possess multiple reactions during TI stimulation due to the complexity of neural responses [56]. This indicates that the response of neurons to TI stimulation may not be limited to one single result but instead encompass various patterns and states of response. Further research is required to enhance the utilized model in this study towards more comprehensive models to better understand the mechanism of TI stimulation.

To assess the efficacy of TI stimulation from a clinical point of view, the crucial factors of electrode placement, difference frequency, and current ratio play a pivotal role in achieving the desired level of stimulation depth within the brain. To do this, the second part of the study involved an experimental test conducted on an anesthetized rat to investigate the impact of TI stimulation on the

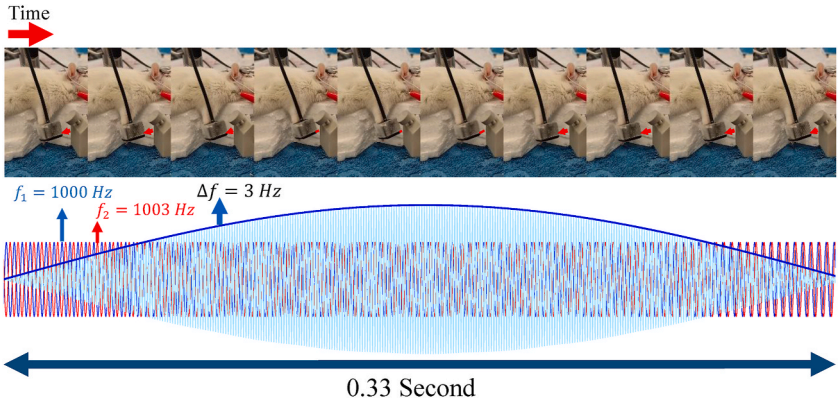

Fig. 6. 10 shots of the movement of the right hand in 0.33 s during TI stimulation of the rat motor cortex with the intensity of $I_1 = I_2 = 2mA$, a carrier frequency of 1000 Hz, and a difference frequency of 3 Hz.

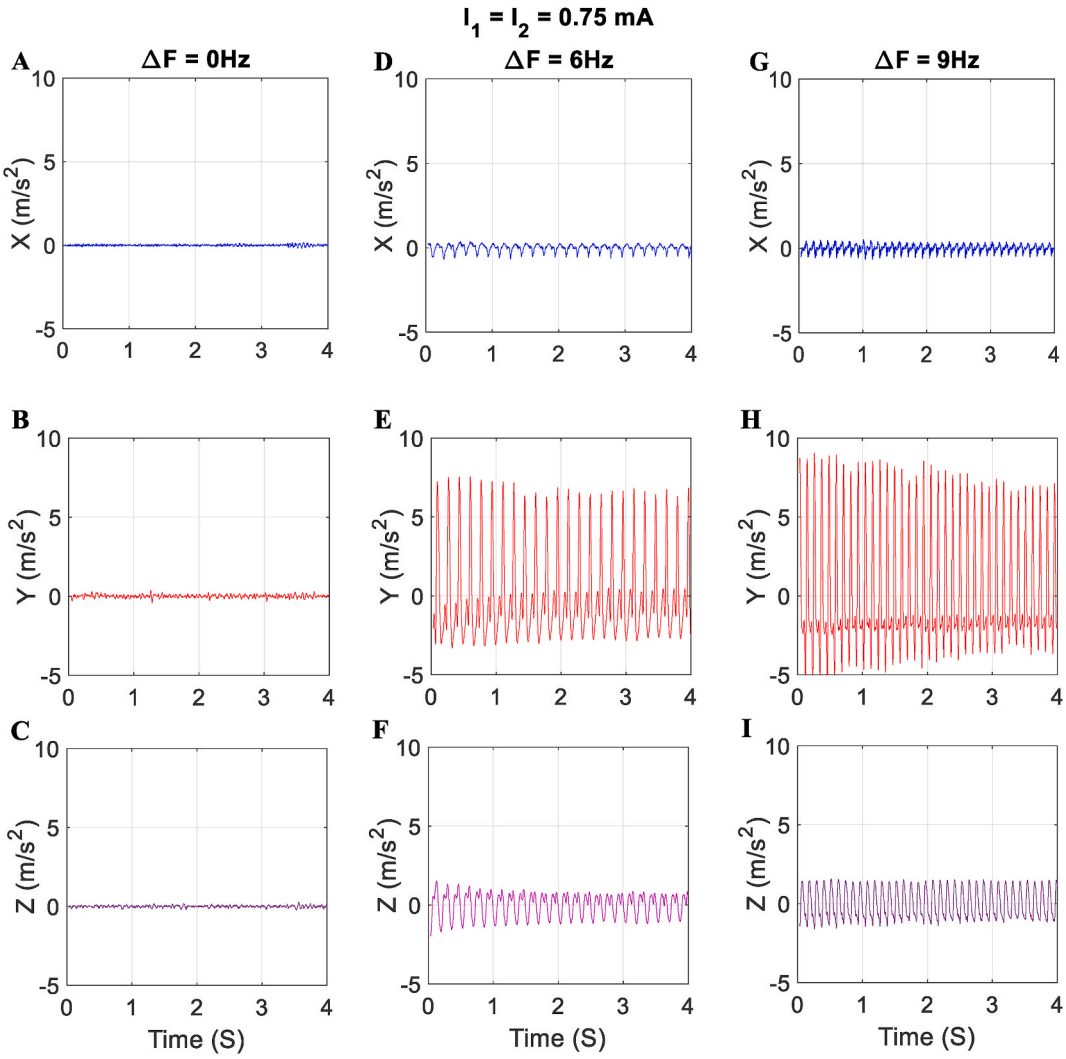

Fig. 7. The effect of the difference frequency on the acceleration of the rat's right-hand movement. (A–C) Acceleration signals in x, y, and z directions for Δf = 0 Hz. (D–F) Acceleration signals in x, y, and z directions for Δf = 6 Hz. (G–I) Acceleration signals in x, y, and z directions for Δf = 9 Hz.

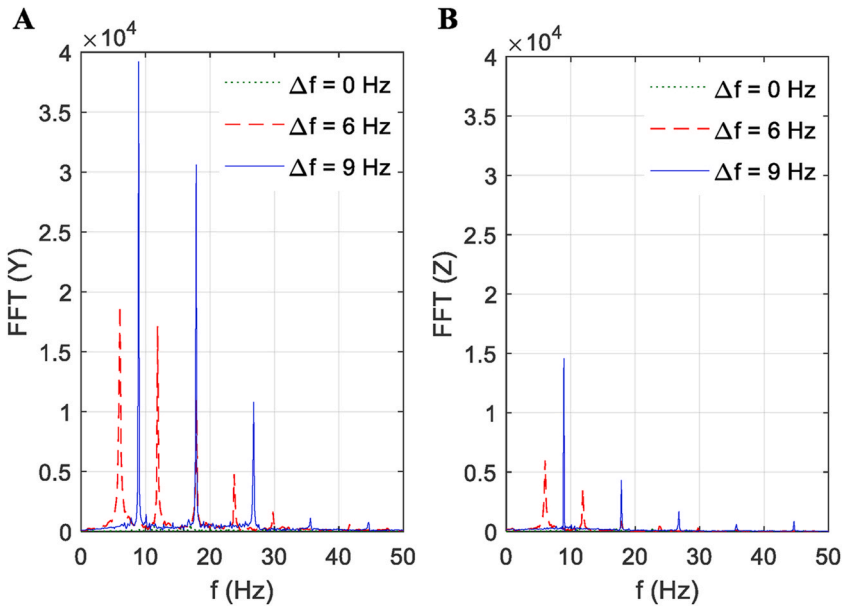

Fig. 8. The frequency spectrum of the rat's hand movement acceleration for $\Delta f = 0$ Hz, $\Delta f = 6$ Hz, and $\Delta f = 9$ Hz in (A) Y direction and (B) Z direction.

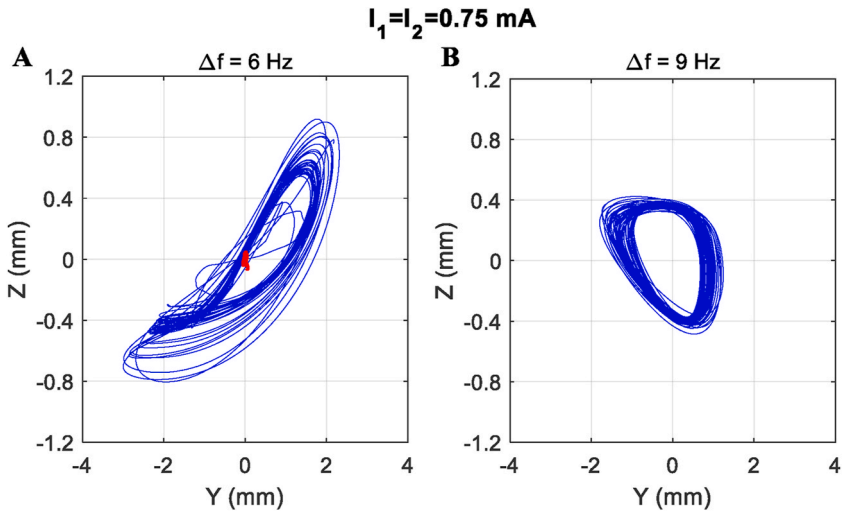

Fig. 9. Position of the rat's right hand affected by the TI stimulation with $I_1 = I_2 = 0.75$ mA. (A) Δf = 6 Hz. (B) Δf = 9 Hz.

activation of the motor cortex using a three axes accelerometer affixed to the right hand of the rat. The results demonstrated that when equal currents were applied to both channels of the TI stimulation, movement of the right hand was detected in the accelerometer signals. These findings were in contrast to the results presented in Ref. [24] which indicated that symmetrical placement of electrodes on the rat's head with balanced currents ($I_1/I_2 = 1$), does not lead to activate the primary motor cortex and generate movement in the rat's hand. This discrepancy can be attributed to the difference in the electrode placement on the rat's head. As detailed in the experimental setup of this study, the common ground electrode was positioned on the left hemisphere causing the envelope modulation peak to deviate towards this hemisphere, even in the balanced scenario. Furthermore, the study examined the effects of unbalanced TI on the rat hand movement. Grossman et al. [24] observed that with unbalanced stimulation (i.e. $I_1 \neq I_2$), the interfering region shifts towards the electrode pair with the lower current. In the current study, to redirect the peak envelope modulation towards the left/right hemisphere, the current ratio of the electrode pairs was modified while keeping the sum of the currents constant. The displacement of the interfering regions was confirmed through the observation of the movement in the contralateral limb. The results indicated no noticeable hand movement when I_1 (right electrode pair) $> I_2$ (left electrode pair), while movement in both y and z directions was detected when $I_1 < I_2$. In the literature, it has been demonstrated that the difference frequency affects the spatial

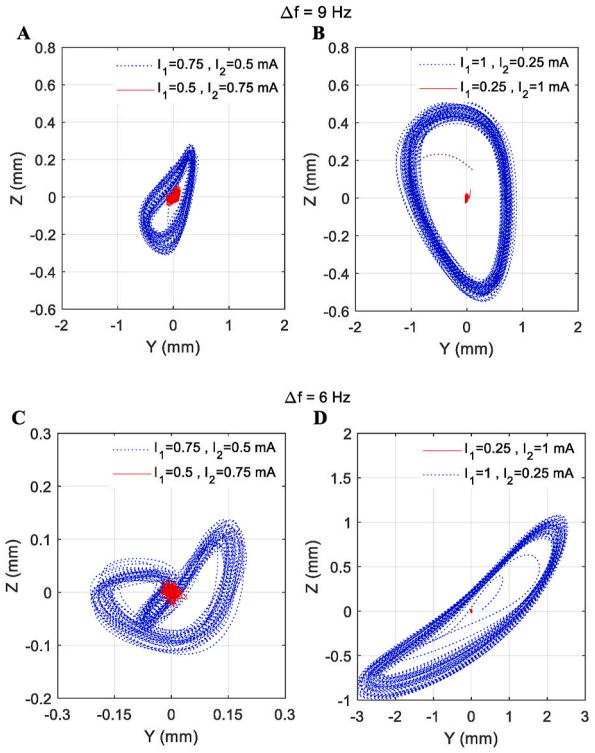

Fig. 10. The effect of the unbalanced TI stimulation on the rat's hand movement. (A) Position of the rat's right hand for I_1:I_2 = 0.75:0.5 mA and I_1:I_2 = 0.5:0.75 mA with Δf = 9 Hz. (B) Position of the rat's right hand for I_1:I_2 = 1:0.25 mA and I_1:I_2 = 0.25:1 mA with Δf = 9 Hz. (C) Position of the rat's right hand for I_1:I_2 = 0.75:0.5 mA and I_1:I_2 = 0.5:0.75 mA with Δf = 6 Hz. (D) Position of the rat's right hand for I_1:I_2 = 1:0.25 mA and I_1:I_2 = 0.25:1 mA with Δf = 6 Hz.

distribution and penetration depth of the electric field generated by the overlapping currents. Understanding the importance of the difference frequency in TI stimulation can help in designing more effective and targeted stimulation protocols to activate deep brain regions. Previous research has indeed explored the impact of electrical stimulation with difference frequencies higher than 100 Hz on the subthalamic nucleus (STN) of the human [57]. The findings have suggested that higher frequencies can potentially be beneficial in the treatment of Parkinson's disease. From a different perspective, in the current study, we evaluated only the effects of stimulation at lower frequencies (6 and 9 Hz) on the amplitude of the generated movement. While the preclinical approaches provide potential therapeutic insights for treating Parkinson's disease, it is important to conduct further research to better understand the mechanisms underlying motor cortex stimulation using TI with high difference frequencies and its potential clinical applications in the treatment of movement disorders including Parkinson's.

The experimental tests in this study were performed on a rat. It is worth noting that, from a statistical point of view, obtaining reliable results in an experimental test requires the repetition of the measurement process. These repetitions can be carried out either over time or across different rats. In the current study, the tests on animal models were repeated over time; however, the investigation was conducted on a single rat. Although the obtained results were entirely consistent with previous studies in the field, it is recommended to replicate the tests on a larger population of rats in order to enhance the reliability of the findings. By doing so, additional factors can be assessed, such as the sensitivity of the range of motion to the difference frequency of the TI stimulation, as well as verifying the reproducibility of the results. Additionally, for a quantitative evaluation of TI stimulation, it is suggested to measure muscle activities using electromyography (EMG) signals and analyze the correlation between the EMG data and the stimulation parameters. In this paper, we investigated the effect of TI stimulation on the activation of the motor cortex in a depth of 3 mm of the cerebral cortex [51]. Recently, Qiu et al., have examined this stimulation technique on the activation of the human motor cortex [30]. Due to the fact that different neural disorders involve specific regions or circuits within the brain, spatially precise stimulation allows clinicians to precisely target the affected brain areas, ensuring that the therapeutic effects are focused on the intended regions. This targeting is crucial for maximizing treatment efficacy while minimizing potential side effects. In the context of clinical application of TI stimulation, one important challenge is achieving the optimal depth of stimulation with a high spatial resolution. To resolve this limitation, by positioning more electrodes on the skull, it may be possible to achieve focused stimulation with higher resolution in deeper areas of the brain [26]. Therefore, future researches should focus on considering the effect of increasing the number of electrode pairs to activate deeper and smaller brain regions. The investigation of the efficacy of TI stimulation specifically focused on the different nuclei in the reward system of the brain for the treatment of cognitive disorders, including morphine addiction in animal models constitutes our current research.

Funding

This research received no external funding.

Institutional review Board Statement

All surgical procedures described in this paper were approved by the Research and Ethics Committee of Isfahan University of Medical Sciences, Isfahan, Iran (No. IR.MUI.AEC.1401.010).

The acceleration dataset used in the current study is available from the corresponding author on reasonable request.

CRediT authorship contribution statement

Zohre Mojiri: Writing – review & editing, Writing – original draft, Visualization, Validation, Supervision, Software, Methodology, Investigation, Formal analysis. **Amir Akhavan:** Writing – review & editing, Writing – original draft, Visualization, Validation, Supervision, Methodology, Investigation, Formal analysis, Conceptualization. **Ehsan Rouhani:** Writing – review & editing, Writing – original draft, Visualization, Validation, Supervision, Methodology, Investigation, Formal analysis, Conceptualization. **Sayed Jalal Zahabi:** Writing – review & editing, Visualization, Validation, Supervision.

Declaration of competing interest

The authors declare that they have no known competing financial interests or personal relationships that could have appeared to influence the work reported in this paper.

Appendix A. Supplementary data

Supplementary data to this article can be found online at https://doi.org/10.1016/j.heliyon.2024.e29482.

References

[1] A.H. Moffa, D. Martin, A. Alonzo, D. Bennabi, D.M. Blumberger, I.M. Benseñor, Z. Daskalakis, F. Fregni, E. Haffen, S.H. Lisanby, F. Padberg, U. Palm, L.B. Razza, B. Sampaio-Jr, C. Loo, A.R. Brunoni, Efficacy and acceptability of transcranial direct current stimulation (tDCS) for major depressive disorder: an individual patient data meta-analysis, Prog. Neuro-Psychopharmacology Biol. Psychiatry 99 (2020), https://doi.org/10.1016/j.pnpbp.2019.109836.

[2] Y. Luo, Y. Sun, X. Tian, X. Zheng, X. Wang, W. Li, X. Wu, B. Shu, W. Hou, Deep brain stimulation for Alzheimer's disease: stimulation parameters and potential mechanisms of action, Front. Aging Neurosci. 13 (2021), https://doi.org/10.3389/fnagi.2021.619543.

[3] Z. Lin, C. Zhang, D. Li, B. Sun, Lateralized effects of deep brain stimulation in Parkinson's disease: evidence and controversies, Npj Park. Dis. 7 (2021), https://doi.org/10.1038/s41531-021-00209-3.

[4] M. Kallupi, J. Kononoff, P.A. Melas, J.S. Qvist, G. de Guglielmo, E.R. Kandel, O. George, Deep brain stimulation of the nucleus accumbens shell attenuates cocaine withdrawal but increases cocaine self-administration, cocaine-induced locomotor activity, and GluR1/GluA1 in the central nucleus of the amygdala in male cocaine-dependent rats, Brain Stimul. 15 (2022) 13–22, https://doi.org/10.1016/j.brs.2021.11.003.

[5] H.R. Siebner, K. Funke, A.S. Aberra, A. Antal, S. Bestmann, R. Chen, J. Classen, M. Davare, V. Di Lazzaro, P.T. Fox, M. Hallett, A.N. Karabanov, J. Kesselheim, M. M. Beck, G. Koch, D. Liebetanz, S. Meunier, C. Miniussi, W. Paulus, A.V. Peterchev, T. Popa, M.C. Ridding, A. Thielscher, U. Ziemann, J.C. Rothwell, Y. Ugawa, Transcranial magnetic stimulation of the brain: what is stimulated? – a consensus and critical position paper, Clin. Neurophysiol. 140 (2022) 59–97, https://doi.org/10.1016/j.clinph.2022.04.022.

[6] T. Reed, R. Cohen Kadosh, Transcranial electrical stimulation (tES) mechanisms and its effects on cortical excitability and connectivity, J. Inherit. Metab. Dis. 41 (2018) 1123–1130, https://doi.org/10.1007/s10545-018-0181-4.

[7] E. Acerbo, A. Jegou, C. Luff, P. Dzialecka, B. Botzanowski, F. Missey, I. Ngom, S. Lagarde, F. Bartolomei, A. Cassara, E. Neufeld, V. Jirsa, R. Carron, N. Grossman, A. Williamson, Focal non-invasive deep-brain stimulation with temporal interference for the suppression of epileptic biomarkers, Front. Neurosci. 16 (2022), https://doi.org/10.3389/fnins.2022.945221.

[8] J.K. Krauss, N. Lipsman, T. Aziz, A. Boutet, P. Brown, J.W. Chang, B. Davidson, W.M. Grill, M.I. Hariz, A. Horn, M. Schulder, A. Mammis, P.A. Tass, J. Volkmann, A.M. Lozano, Technology of deep brain stimulation: current status and future directions, Nat. Rev. Neurol. 17 (2021) 75–87, https://doi.org/10.1038/s41582-020-00426-z.

[9] H. Sharma, V.Y. Vishnu, N. Kumar, V. Sreenivas, M.R. Rajeswari, R. Bhatia, R. Sharma, M.V.P. Srivastava, Efficacy of low-frequency repetitive transcranial magnetic stimulation in ischemic stroke: a double-blind randomized controlled trial, Arch. Rehabil. Res. Clin. Transl. 2 (2020) 100039, https://doi.org/10.1016/j.arrct.2020.100039.

[10] T.A. Low, K. Lindland, A. Kirton, H.L. Carlson, A.D. Harris, B.G. Goodyear, O. Monchi, M.D. Hill, S.P. Dukelow, Repetitive transcranial magnetic stimulation (rTMS) combined with multi-modality aphasia therapy for chronic post-stroke non-fluent aphasia: a pilot randomized sham-controlled trial, Brain Lang. 236 (2023) 105216, https://doi.org/10.1016/j.bandl.2022.105216.

[11] T.M. Mi, S. Garg, F. Ba, A.P. Liu, P.P. Liang, L.L. Gao, Q. Jia, E.H. Xu, K.C. Li, P. Chan, M.J. McKeown, Repetitive transcranial magnetic stimulation improves Parkinson's freezing of gait via normalizing brain connectivity, Npj Park. Dis. 6 (2020), https://doi.org/10.1038/s41531-020-0118-0.

[12] M.F. Gwynette, D.W. Lowe, E.A. Henneberry, G.L. Sahlem, M.G. Wiley, H. Alsarraf, S.B. Russo, J.E. Joseph, P.M. Summers, L. Lohnes, M.S. George, Treatment of adults with autism and major depressive disorder using transcranial magnetic stimulation: an open label pilot study, Autism Res. 13 (2020) 346–351, https://doi.org/10.1002/aur.2266.

[13] X. Li, C. Yu, Y. Ding, Z. Chen, W. Zhuang, Z. Liu, J. Fan, H. Yan, W. Xu, G. Zhu, X. Zhang, D. Zhou, Motor cortical plasticity as a predictor of treatment response to high frequency repetitive transcranial magnetic stimulation (rTMS) for cognitive function in drug-naive patients with major depressive disorder, J. Affect. Disord. 334 (2023) 180–186, https://doi.org/10.1016/j.jad.2023.04.085.

[14] D.S. Santos, L.F. Medeiros, D.J. Stein, I.C. De Macedo, D.E. Da Silva Rios, C. De Oliveira, R.S. Toledo, F. Fregni, W. Caumo, I.L.S. Torres, Bimodal transcranial direct current stimulation reduces alcohol consumption and induces long-term neurochemical changes in rats with neuropathic pain, Neurosci. Lett. 759 (2021), https://doi.org/10.1016/j.neulet.2021.136014.

[15] G.G. Regner, P. Pereira, D.T. Leffa, C. de Oliveira, R. Vercelino, F. Fregni, I.L.S. Torres, Preclinical to clinical translation of studies of transcranial direct-current stimulation in the treatment of epilepsy: a systematic review, Front. Neurosci. 12 (2018), https://doi.org/10.3389/fnins.2018.00189.

[16] A.S. Coles, K. Kozak, T.P. George, A review of brain stimulation methods to treat substance use disorders, Am. J. Addict. 27 (2018) 71–91, https://doi.org/10.1111/ajad.12674.

[17] Z. Rezaei, H. Alaei, P. Reisi, Effects of electrical stimulation and temporary inactivation of basolateral amygdala on morphine-induced conditioned place preference in rats, Neurosci. Lett. 774 (2022), https://doi.org/10.1016/j.neulet.2022.136519.

[18] Z. Jokar, S. Khatamsaz, H. Alaei, M. Shariati, The electrical stimulation of the central nucleus of the amygdala in combination with dopamine receptor antagonist reduces the acquisition phase of morphine-induced conditioned place preference in male rat, Res. Pharm. Sci. 18 (2023) 430–438, https://doi.org/10.4103/1735-5362.378089.

[19] L.A. Johnson, J. Wang, S.D. Nebeck, J. Zhang, M.D. Johnson, J.L. Vitek, Direct activation of primary motor cortex during subthalamic but not pallidal deep brain stimulation, J. Neurosci. 40 (2020) 2166–2177, https://doi.org/10.1523/JNEUROSCI.2480-19.2020.

[20] S. Smeets, A. Boogers, T. Van Bogaert, J. Peeters, M. McLaughlin, B. Nuttin, T. Theys, W. Vandenberghe, P. De Vloo, Deep brain stimulation with short versus conventional pulse width in Parkinson's disease and essential tremor: a systematic review and meta-analysis, Brain Stimul. 17 (2023) 71–82, doi: 10.1016/j.brs.2023.12.013..

[21] A.T. Hale, M.A. Monsour, J.D. Rolston, R.P. Naftel, D.J. Englot, Deep brain stimulation in pediatric dystonia: a systematic review, Neurosurg. Rev. 43 (2020), https://doi.org/10.1007/s10143-018-1047-9.

[22] P.S. Larson, Deep brain stimulation for movement disorders, Neurotherapeutics 11 (2014) 465–474, https://doi.org/10.1007/s13311-014-0274-1.

[23] X. Liu, F. Qiu, L. Hou, X. Wang, Review of noninvasive or minimally invasive deep brain stimulation, Front. Behav. Neurosci. 15 (2022), https://doi.org/10.3389/fnbeh.2021.820017.

[24] N. Grossman, D. Bono, N. Dedic, S.B. Kodandaramaiah, A. Rudenko, H.J. Suk, A.M. Cassara, E. Neufeld, N. Kuster, L.H. Tsai, A. Pascual-Leone, E.S. Boyden, Noninvasive deep brain stimulation via temporally interfering electric fields, Cell 169 (2017), https://doi.org/10.1016/j.cell.2017.05.024, 1029-1041.e16.

[25] F. Karimi, A. Attarpour, R. Amirfattahi, A.Z. Nezhad, Computational analysis of non-invasive deep brain stimulation based on interfering electric fields, Phys. Med. Biol. 64 (2019), https://doi.org/10.1088/1361-6560/ab5229.

[26] Q. Xiao, Z. Zhong, X. Lai, H. Qin, A multiple modulation synthesis method with high spatial resolution for noninvasive neurostimulation, PLoS One 14 (2019) 1–15, https://doi.org/10.1371/journal.pone.0218293.

[27] F. Missey, M.S. Ejneby, I. Ngom, M.J. Donahue, J. Trajlinek, E. Acerbo, B. Botzanowski, A.M. Cassarà, E. Neufeld, E.D. Głowacki, L. Shangold, W.M. Hanes, A. Williamson, Obstructive sleep apnea improves with non-invasive hypoglossal nerve stimulation using temporal interference, Bioelectron. Med. 9 (2023), https://doi.org/10.1186/s42234-023-00120-7.

[28] I. Violante, K. Alania, A. Cassarà, E. Neufeld, E. Acerbo, A. Williamson, D. Kurtin, E. Rhodes, A. Hampshire, N. Kuster, E. Boyden, A. Pascual-Leone, N. Grossman, Non-invasive temporal interference electrical stimulation of the human hippocampus, Brain Stimul. 16 (2023) 408, https://doi.org/10.1016/j.brs.2023.01.833.

[29] M.J. Wessel, E. Beanato, T. Popa, F. Windel, P. Vassiliadis, P. Menoud, V. Beliaeva, I.R. Violante, H. Abderrahmane, P. Dzialecka, C.-H. Park, P. Maceira-Elvira, T. Morishita, A. Cassara, M. Steiner, N. Grossman, E. Neufeld, F.C. Hummel, Noninvasive theta-burst stimulation of the human striatum enhances striatal activity and motor skill learning, Nat. Neurosci. 26 (2023) 2005–2016, https://doi.org/10.1038/s41593-023-01457-7.

[30] R. Ma, X. Xia, W. Zhang, Z. Lu, Q. Wu, J. Cui, H. Song, C. Fan, X. Chen, R. Zha, J. Wei, G.J. Ji, X. Wang, B. Qiu, X. Zhang, High gamma and beta temporal interference stimulation in the human motor cortex improves motor functions, Front. Neurosci. 15 (2022), https://doi.org/10.3389/fnins.2021.800436.

[31] F. Missey, E. Rusina, E. Acerbo, B. Botzanowski, A. Trébuchon, F. Bartolomei, V. Jirsa, R. Carron, A. Williamson, Orientation of temporal interference for non-invasive deep brain stimulation in epilepsy, Front. Neurosci. 15 (2021), https://doi.org/10.3389/fnins.2021.633988.

[32] F. Missey, M.J. Donahue, P. Weber, I. Ngom, E. Acerbo, B. Botzanowski, L. Migliaccio, V. Jirsa, E.D. Głowacki, A. Williamson, Laser-driven wireless deep brain stimulation using temporal interference and organic electrolytic photocapacitors, Adv. Funct. Mater. 32 (2022), https://doi.org/10.1002/adfm.202200691.

[33] X. Su, J. Guo, M. Zhou, J. Chen, L. Li, Y. Chen, X. Sui, H. Li, X. Chai, Computational modeling of spatially selective retinal stimulation with temporally interfering electric fields, IEEE Trans. Neural Syst. Rehabil. Eng. 29 (2021) 418–428, https://doi.org/10.1109/TNSRE.2021.3055203.

[34] J. Gomez-Tames, A. Asai, A. Hirata, Multiscale computational model Reveals nerve response in a mouse model for temporal interference brain stimulation, Front. Neurosci. 15 (2021), https://doi.org/10.3389/fnins.2021.684465.

[35] Z. Esmaeilpour, G. Kronberg, D. Reato, L.C. Parra, M. Bikson, Temporal interference stimulation targets deep brain regions by modulating neural oscillations, Brain Stimul. 14 (2021) 55–65, https://doi.org/10.1016/j.brs.2020.11.007.

[36] R. Cubo, M. Aström, A. Medvedev, Optimization of lead design and electrode configuration in deep brain stimulation, Int. J. Adv. Life Sci. 8 (2016) 76–86.

[37] S. Lee, C. Lee, J. Park, C.H. Im, Individually customized transcranial temporal interference stimulation for focused modulation of deep brain structures: a simulation study with different head models, Sci. Rep. 10 (2020), https://doi.org/10.1038/s41598-020-68660-5.

[38] M. Åström, E. Diczfalusy, H. Martens, K. Wårdell, Relationship between neural activation and electric field distribution during deep brain stimulation, IEEE Trans. Biomed. Eng. 62 (2015), https://doi.org/10.1109/TBME.2014.2363494.

[39] A.L. Hodgkin, A.F. Huxley, A quantitative description of membrane current and its application to conduction and excitation in nerve, J. Physiol. 117 (1952) 500–544, https://doi.org/10.1113/jphysiol.1952.sp004764.

[40] C. Meunier, I. Segev, Playing the Devil's advocate: is the Hodgkin-Huxley model useful? Trends Neurosci. 25 (2002) 558–563, https://doi.org/10.1016/S0166-2236(02)02278-6.

[41] R.W. Anderson, A.A. Farokhniaee, K. Gunalan, B. Howell, C.C. McIntyre, Action potential initiation, propagation, and cortical invasion in the hyperdirect pathway during subthalamic deep brain stimulation, Brain Stimul. 11 (2018) 1140–1150, https://doi.org/10.1016/j.brs.2018.05.008.

[42] E. Rouhani, Y. Fathi, Robust multi-input multi-output adaptive fuzzy terminal sliding mode control of deep brain stimulation in Parkinson's disease: a simulation study, Sci. Rep. 11 (2021), https://doi.org/10.1038/s41598-021-00365-9.

[43] E. Rouhani, E. Jafari, A. Akhavan, Suppression of seizure in childhood absence epilepsy using robust control of deep brain stimulation: a simulation study, Sci. Rep. 13 (2023), https://doi.org/10.1038/s41598-023-27527-1.

[44] M. Khodashenas, G. Baghdadi, F. Towhidkhah, A modified Hodgkin–Huxley model to show the effect of motor cortex stimulation on the trigeminal neuralgia network, J. Math. Neurosci. 9 (2019), https://doi.org/10.1186/s13408-019-0072-5.

[45] E. Mirzakhalili, B. Barra, M. Capogrosso, S.F. Lempka, Biophysics of temporal interference stimulation, Cell Syst 11 (2020), https://doi.org/10.1016/j.cels.2020.10.004, 557-572.e5.

[46] J. Cao, P. Grover, Do single neuron models exhibit temporal interference stimulation?, in: 2018 IEEE Biomed. Circuits Syst. Conf. BioCAS 2018 - Proc., 2018, https://doi.org/10.1109/BIOCAS.2018.8584745.

[47] N.A. Pelot, W.M. Grill, In vivo quantification of excitation and kilohertz frequency block of the rat vagus nerve, J. Neural. Eng. 17 (2020), https://doi.org/10.1088/1741-2552/ab6cb6.

[48] B. Botzanowski, M.J. Donahue, M.S. Ejneby, A.L. Gallina, I. Ngom, F. Missey, E. Acerbo, D. Byun, R. Carron, A.M. Cassarà, E. Neufeld, V. Jirsa, P.S. Olofsson, E. D. Głowacki, A. Williamson, Noninvasive stimulation of peripheral nerves using temporally-interfering electrical fields, Adv. Healthc. Mater. 11 (2022), https://doi.org/10.1002/adhm.202200075.

[49] N. Grossman, M.S. Okun, E.S. Boyden, Translating temporal interference brain stimulation to treat neurological and psychiatric conditions, JAMA Neurol. 75 (2018) 1307–1308, https://doi.org/10.1001/jamaneurol.2018.2760.

[50] M. Pospischil, M. Toledo-Rodriguez, C. Monier, Z. Piwkowska, T. Bal, Y. Frégnac, H. Markram, A. Destexhe, Minimal Hodgkin-Huxley type models for different classes of cortical and thalamic neurons, Biol. Cybern. 99 (2008) 427–441, https://doi.org/10.1007/s00422-008-0263-8.

[51] G. Paxinos, C. Watson, The Rat Brain in Stereotaxic Coordinates: Hard Cover Edition, Elsevier, 2006.

[52] J. Cao, P. Grover, STIMULUS: noninvasive dynamic patterns of neurostimulation using Spatio-temporal interference, IEEE Trans. Biomed. Eng. 67 (2020) 726–737, https://doi.org/10.1109/TBME.2019.2919912.

[53] N.D. Crosby, J.J. Janik, W.M. Grill, Modulation of activity and conduction in single dorsal column axons by kilohertz-frequency spinal cord stimulation, J. Neurophysiol. 117 (2017) 136–147, https://doi.org/10.1152/jn.00701.2016.
[54] S.F. Lempka, C.C. McIntyre, K.L. Kilgore, A.G. Machado, Computational analysis of kilohertz frequency spinal cord stimulation for chronic pain management, Anesthesiology (2015) 1362–1376, https://doi.org/10.1097/ALN.0000000000000649.
[55] N. Bhadra, E.A. Lahowetz, S.T. Foldes, K.L. Kilgore, Simulation of high-frequency sinusoidal electrical block of mammalian myelinated axons, J. Comput. Neurosci. 22 (2007) 313–326, https://doi.org/10.1007/s10827-006-0015-5.
[56] J.D. Johansson, Estimation of electric field impact in deep brain stimulation from axon diameter distribution in the human brain, Biomed, Phys. Eng. Express 7 (2021), https://doi.org/10.1088/2057–1976/ac2dd4.
[57] M. Rizzone, M. Lanotte, B. Bergamasco, A. Tavella, E. Torre, G. Faccani, A. Melcarne, L. Lopiano, Deep brain stimulation of the subthalamic nucleus in Parkinson's disease: effects of variation in stimulation parameters, J. Neurol. Neurosurg. Psychiatry 71 (2001) 215–219, https://doi.org/10.1136/jnnp.71.2.215.